

Anomalous Relationship between Molecular Size and Diffusivity of Ethane and Ethylene inside Crystals of Zeolitic Imidazolate Framework-11

Amineh Baniani,[†] Christian Chmelik,[‡] Evan M. Forman,[†] Lei Fan,[†] Erkang Zhou,[§] Fengyi Zhang,[§] Richelle Lyndon,[§] Ryan P. Lively,[§] and Sergey Vasenkov^{*,†,§}

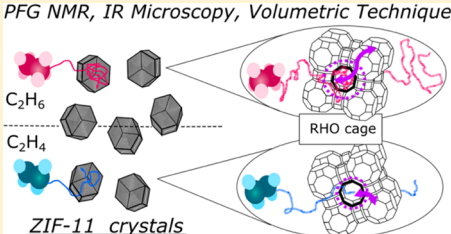
[†]Department of Chemical Engineering, University of Florida, Gainesville, Florida 32611, United States

[‡]Faculty of Physics and Earth Sciences, Leipzig University, Linnéstraße 5, D-04103 Leipzig, Germany

[§]School of Chemical & Biomolecular Engineering, Georgia Institute of Technology, Atlanta, Georgia 30332, United States

Supporting Information

ABSTRACT: Multinuclear pulsed field gradient (PFG) NMR was used to study the self-diffusion of ethane and ethylene inside loosely packed beds of zeolitic imidazolate framework-11 (ZIF-11) crystals. Diffusion measurements were performed at different temperatures under conditions where the length scales of displacements were smaller than or comparable with the mean size of the ZIF-11 crystals. For the crystal beds loaded with a single sorbate, these studies showed a larger intracrystalline diffusivity for ethane than that for ethylene under the same or comparable experimental conditions, an unexpected result due to the larger size of ethane compared to that of ethylene. PFG NMR diffusion studies of ZIF-11 beds loaded with ethane/ethylene mixtures revealed that substituting a fraction of ethane molecules by ethylene molecules decreases the intracrystalline diffusivity of ethane. These results in combination with an observation of a higher-for-ethylene-than-for-ethane activation energy of intracrystalline self-diffusion in single-sorbate systems suggest a hindering effect of ethylene molecules on the intra-ZIF diffusion. To further confirm and investigate the anomalous relationship between ethane and ethylene intracrystalline diffusivities in ZIF-11, uptake curves for ethane and ethylene were measured in single crystals using IR microscopy and in a thin crystal bed using a volumetric technique. The diffusion data obtained from these complementary uptake studies under the same or comparable conditions were found to be consistent with the PFG NMR measurements. The observed anomalous relationship between ethane and ethylene diffusivities in ZIF-11 is discussed in the context of the flexibility of the ZIF-11 framework.



INTRODUCTION

Zeolitic imidazolate frameworks (ZIFs) represent a subclass of metal–organic frameworks (MOFs) with zeolite-like topologies. ZIFs are promising materials for application in gas separation due to their large porosity, outstanding chemical and thermal stabilities, and well-defined pores with sizes in the range of 0.2–2 nm.^{1–5} Most importantly, the pore and pore aperture sizes of ZIFs can be tuned to achieve selective molecular sieving.^{4,6,7} It is well known that for many ZIF types, the framework flexibility of these materials allows molecules with sizes larger than a ZIF pore aperture size to enter and diffuse inside ZIF pore systems (see, for example, refs 8–16). Clearly, it is of crucial importance to develop a fundamental understanding of ZIF transport properties and their relationship with the framework flexibility for optimizing applications of ZIFs in gas separations.

Although many different types of ZIFs have been synthesized, until now, a large fraction of the experimental and simulation studies have been performed on ZIF-8 owing to its potential to separate small molecules.^{6,10,12,13,17–20} ZIF-11 is another promising type of ZIFs that has caught the attention of the scientific community for its potential related to gas

separations.²¹ ZIF-11 is composed of benzimidazolate ligands and tetrahedral Zn²⁺ metal centers resulting in RHO topology (Figure S1).³ Compared to ZIF-8, ZIF-11 has similar chemical and thermal stabilities, but its nominal pore aperture size (3.0 Å³) is smaller than that of ZIF-8. In our recent pulsed field gradient (PFG) NMR diffusion study, we have compared the intracrystalline self-diffusivities of a single sorbate (ethylene) in ZIF-11 beds and in ZIF-11 crystals dispersed in different polymer matrices to form mixed-matrix membranes (MMMs). It was found that confining ZIF-11 in a polymer can reduce intra-ZIF self-diffusivity of ethylene.¹¹ This diffusivity reduction effect was attributed to a reduction in ZIF-11 framework flexibility due to confinement in a polymer. The dependence of a sorbate loading on its self-diffusion in ZIF-11 has been studied by a different research group for a single gas (ethane).²² The authors observed a significant reduction in the self-diffusivity with increasing ethane loading. This observation was attributed to a reduction in the linker

Received: April 26, 2019

Revised: June 18, 2019

Published: June 19, 2019

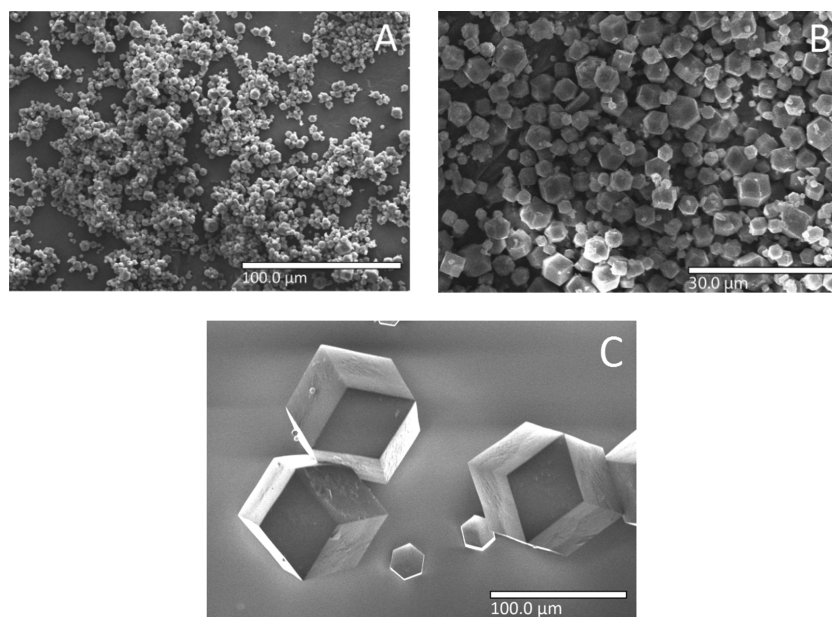


Figure 1. Scanning electron microscopy (SEM) images of small (A, B) and large (C) ZIF-11 crystal batches.

flexibility at high sorbate concentrations.²² It is important to note that the very fact of the diffusion observation for ethane (4.44 Å^{1,23}) and ethylene (4.16 Å^{1,23}) in ZIF-11 (3.0 Å³) represents clear evidence of a large role played by the framework flexibility of ZIF-11 crystals in intracrystalline sorbate diffusion.

The present work focuses on an experimental investigation and understanding of the ethane/ethylene diffusion selectivity, i.e., the ratio of the diffusivity of these sorbates measured in ZIF-11 under the same or similar conditions for pure and mixed gases. Ethane/ethylene mixture is a common industrial paraffin/olefin mixture, where ethylene is required for the production of polyethylene, polystyrene, and other polymers needed in many applications.^{24,25} Diffusion measurements were performed using ¹H and ¹³C PFG NMR at different temperatures and concentrations of mixed and pure gases in batches of small (3.1 and 4.5 μm) and large (100 μm) ZIF-11 crystals. The PFG NMR studies benefited from a combination of high-field (17.6 or 14 T) and high-magnetic-field gradients (up to 25 T/m), which allowed obtaining self-diffusivities for the length scales of displacements smaller than the mean crystal size even in the small crystal batches suitable for the MMM formation. The 100 μm batch was used to enable complementary studies of ethane and ethylene diffusion in ZIF-11 crystals using two other techniques, which require large crystal size under our measurement conditions: infrared microscopy (IRM) and volumetric uptake technique. The reported diffusion data indicate that ethylene diffuses at a slower rate compared to ethane in ZIF-11 crystals despite its smaller molecular size compared to ethane. The observed satisfactory agreement between the diffusion data measured by ¹H PFG NMR, ¹³C PFG NMR, IR microscopy, and volumetric uptake under the same or similar experimental conditions confirms the absence of any measurement artifacts. The data are discussed in the context of the flexibility of the ZIF-11 framework.

EXPERIMENTAL SECTION

Materials. All chemicals were used without further purification. Benzimidazole and zinc acetate dihydrate were purchased from Alfa Aesar. Zinc bromide dihydrate was purchased from Sigma-Aldrich. Methanol and toluene were purchased from VWR International. Ammonium hydroxide solutions were purchased from BDH Chemicals. For the uptake and adsorption isotherm measurements, ethane (99.99%) was purchased from Airgas and ethylene (99.99%) was purchased from Matheson. The sorbates used for PFG NMR studies were ¹³C₁-enriched ethane consisting of a 99% isotopic purity (Sigma-Aldrich), ¹³C₂-enriched ethane consisting of a 99% isotopic purity (Sigma-Aldrich), and ¹³C₂-enriched ethylene consisting of a 99% isotopic purity (Sigma-Aldrich).

ZIF-11 Synthesis. Small ZIF-11 crystals were synthesized via solvothermal method.²⁶ Benzimidazole (0.6 g, 5 mmol) was dissolved in 21 mL of methanol and 3.8 mL of ammonium hydroxide solution (18%). To this, a solution of zinc acetate (0.55 g, 2.5 mmol) in 21 mL of methanol and 15 mL of toluene was added. The reaction mixture was stirred for 2 h at room temperature. The ZIF-11 crystals were recovered by vacuum filtration, washed with methanol, and activated at 403 K under vacuum for 24 h (Figure 1A,B).

The synthesis of larger ZIF-11 crystals (~100 μm) was modified from a previously reported procedure.²⁶ Zinc bromide (0.13 g, 0.5 mmol) was dissolved in 4 mL of methanol and 3 mL of toluene. A solution of benzimidazole (0.059 g, 0.5 mmol) in 4.2 mL of methanol and 0.8 mL of ammonium hydroxide (30%) was added to the zinc solution. The reaction mixture was mixed briefly and then left undisturbed for 4 days at room temperature. The crystals were washed, and the solvent was exchanged three times a day for 2 days with methanol and activated at 403 K under vacuum overnight (Figure 1C). The crystals were sieved through a 106 μm sized mesh to remove most of the smaller ZIF-11 crystals.

Particle size distributions of the ZIF-11 crystals are characterized by SEM and analyzed by ImageJ (Figures 1 and S2; Table S1). The measured powder X-ray diffraction

Table 1. Loading Pressure and Respective Concentration of Ethane and Ethylene in the ZIF-11 Bed Samples As Measured Using NMR Signal Analysis

sample	ethane loading pressure ^a (bar)	ethane loading ^b (mmol/g)	ethylene loading pressure ^a (bar)	ethylene loading ^b (mmol/g)
ZIF-11 bed (single gas)	0.1	0.36	0.1	0.32
ZIF-11 bed (single gas)	0.3	0.62	0.3	0.60
ZIF-11 bed (single gas)	0.6	0.80	0.6	0.87
ZIF-11 bed (single gas)	0.8	1.4	0.8	1.2
ZIF-11 bed (single gas)	2.1	2.0	2.0	1.7
ZIF-11 bed (single gas)	9.0	2.7	9.0	2.8
ZIF-11 bed (single gas)	9.1	3.0	9.1	3.1
ZIF-11 bed (gas mixture)	1.1	0.90	1.2	0.73
ZIF-11 bed (gas mixture)	4.0	2.0	3.9	2.0

^a15% experimental uncertainty. ^b20% experimental uncertainty.

pattern (Figure S3) was found to be in agreement with the corresponding simulated pattern of ZIF-11.

Preparation of NMR Samples. Standard 5 mm NMR tubes (Wilma-LabGlass) were filled with loosely packed beds of ZIF-11 crystals up to a height between around 10 and 24 mm, depending on the amount of the material available from a particular batch. Samples were activated (i.e., made sorbate-free) using a custom-made vacuum system by keeping the samples under high vacuum overnight at 423 K. Upon activation, the samples were allowed to cool down to 298 K and loaded with sorbate(s). Pure C₂H₆ and C₂H₄, as well as C₂H₆/C₂H₄ mixtures, were loaded into the samples by cryogenically condensing the desired amounts into the NMR tubes with the ZIF-11 beds using liquid nitrogen. The tubes were flame-sealed upon sorbate loading and separated from the vacuum system. Samples requiring small sorbate loadings corresponding to sorbate loading pressures of less than 1 bar were also loaded by exposing the crystal bed in the NMR tube to the sorbate (ethane or ethylene) at the desired loading pressure and 296 K for at least 2 h, the loading time after which no changes in the amount adsorbed were observed based on the measured NMR signal of the respective sorbate. The sample tubes were flame-sealed upon loading.

The sorbate loadings in each material were determined by comparing the NMR signal of the sorbate (ethane or ethylene) in the studied samples with the NMR signal of the corresponding bulk gas at a known pressure in a similar way, as discussed in ref 27. For the samples loaded by cryogenic condensation, the following additional procedure was used. Sealed NMR tubes with a porous sample were placed upside down (gas-filled volume is below the porous material) to measure the NMR signal from the gas phase of the NMR tube. A gas-permeable Doty susceptibility plug (Wilma-LabGlass, Inc.) was placed inside the NMR tubes to prevent ZIF-11 crystals from falling down. NMR signal of the gas region of the samples was compared to that of the reference sample containing the same gas (ethane or ethylene) at a known pressure (no porous material added) to obtain sorbate pressure in the gas phase of the samples with ZIF-11 beds. Sorbate loadings inside ZIF-11 crystals were obtained by subtracting the amount of gas in the gas phase of a sample tube from the known total amount of gas in the sample tube. In the same manner, sorbate loadings of ethane/ethylene mixture were determined as well. Table 1 shows the loading pressure and respective sorbate loadings obtained this way for each studied sample. For pure gases, it was verified that the loading data obtained by NMR are in agreement, within uncertainty, with

the results of the standard adsorption isotherm measurements (Figure S4).

NMR Measurements. PFG NMR diffusion measurements were performed using a 17.6 T Avance III HD spectrometer (Bruker BioSpin) and 14 T Avance III spectrometer (Bruker BioSpin) operating at resonance frequencies of 750 and 600 MHz for ¹H and 188.6 and 149.8 MHz for ¹³C, respectively. Sine-shaped and trapezoidal-shaped, bipolar magnetic field gradients with the effective duration of 2–2.5 ms and amplitudes of up to 25 and 18 T/m were generated using Diff50 and Diff30 diffusion probes (Bruker BioSpin), respectively. The reported NMR data were obtained after keeping the samples at a chosen temperature inside the magnet for a minimum of 1 h to ensure the sorption equilibrium conditions in the sample. Standard adsorption isotherm measurements confirmed that such equilibration time is sufficient. Furthermore, the measured NMR signal, which is proportional to the total number of sorbate molecules in the studied ZIF-11 crystal bed, was monitored during the measurements that lasted at least several hours at a constant temperature. No changes in the signal were observed, indicating no change in the gas concentration inside the porous materials. Hence, all reported NMR data correspond to the condition of sorption equilibrium at the temperatures used in this work.

Diffusion measurements were performed using the 13-interval PFG NMR pulse sequence with bipolar gradients,²⁸ modified by the addition of a longitudinal eddy current delay. The effective diffusion time varied between 10 and 270 ms, and the time between the first and second $\pi/2$ radio-frequency pulses of the 13-interval sequence was 8.5 and 3.5 ms for ¹³C and ¹H, respectively. The repetition delay time, i.e., the time delay between the application of the sequence, varied between 1 and 4 s, and the number of scans was 512 and 256 for ¹³C and ¹H, respectively. The number of scans was, in all cases, sufficiently large for the signal-to-noise ratio to be larger than 20 at the largest gradient amplitude. The total experimental time for measuring a single self-diffusion coefficient was between about 2 and 4 h, depending on the experimental conditions. The self-diffusivities were obtained from the measured PFG NMR attenuation curves, i.e., dependencies of the PFG NMR signal intensity on the magnetic field gradient strength (g) with all other pulse sequence parameters held fixed. PFG NMR signal intensities were obtained separately for ethane and ethylene by the integration of the corresponding NMR spectra. Under our measurement conditions, the ¹³C NMR spectra of ethane and ethylene consisted of single, nonoverlapping lines at around 4.0 and

120.5 ppm, respectively. The ^1H NMR spectra of ethane and ethylene consisted of single lines at 1.8 and 6.3 ppm, respectively. Representative examples of ^{13}C and ^1H NMR spectra of ethane and ethylene as single sorbates in the ZIF-11 bed for the lowest loading pressure at 296 K can be seen in Figures S5 and S6. In the case of normal self-diffusion with a single self-diffusion coefficient (D), PFG NMR attenuation curves can be presented as^{29–32}

$$\Psi = \frac{S(g)}{S(g \approx 0)} = \exp(-Dq^2t) \quad (1)$$

where Ψ is the PFG NMR signal attenuation, S is the PFG NMR signal intensity, t is the time of observation of the diffusion process (i.e., diffusion time), and $q = 2\gamma g\delta$, where γ is the gyromagnetic ratio and δ is the effective gradient pulse length. In the case of normal self-diffusion in three dimensions, the mean-square displacement (MSD) is related to D and t by the Einstein relation

$$\langle r^2 \rangle = 6Dt \quad (2)$$

Most of the PFG NMR attenuation curves reported in this work were measured at 17.6 T using ^{13}C nuclei. ^{13}C PFG NMR measurements benefited from larger-for- ^{13}C -than-for- ^1H T_2 NMR relaxation times in the samples studied in this work (Tables S2 and S3). To confirm the absence of magnetic susceptibility effects and/or any other measurement artifacts, complementary diffusion measurements were performed with selected samples under the same measurement conditions using ^1H nuclei at 17.6 T or ^{13}C nuclei at a lower field of 14 T or ^1H nuclei at 14 T. The observed coincidence of the results obtained from the latter measurements with the corresponding data measured with the same samples by ^{13}C PFG NMR at 17.6 T confirmed the absence of any measurement artifacts under our experimental conditions.

The uncertainty of the diffusivities reported in the paper is based on the reproducibility of the diffusion data measured with two to three identically prepared (but different) samples. The uncertainty of the diffusivities is also based on the reproducibility of the data measured with the same samples but at different fields (17.6 and 14 T) and/or using different nuclei types (^{13}C and ^1H).

Longitudinal (T_1) and transverse (T_2) NMR relaxation times were estimated using the 13-interval PFG NMR sequence. For T_1 relaxation times, the measurements were performed by changing the time interval between the second and third $\pi/2$ radio-frequency pulses of the sequence while keeping all other time intervals constant. For T_2 relaxation times, the measurements were performed by changing the time interval between the first and second $\pi/2$ radio-frequency pulses of the sequence. Under the conditions of these measurements, it was ensured that there was no attenuation of the signal due to sorbate diffusion inside ZIF-11 crystals. At the same time, all signal from the gas phase of the sample was completely suppressed by the applied gradients. As a result, the reported T_1 and T_2 relaxation times correspond to the respective sorbates located inside ZIF-11 crystals. The relaxation measurements were performed using the 13-interval PFG NMR sequence because such measurements provide a direct approach to estimate the total loss of the signal in the diffusion measurements due to NMR relaxation. As high magnetic field and complex samples are used, measured NMR relaxation times can depend on the NMR sequence. The

measured T_1 and T_2 relaxation times are presented in Tables S2 and S3. In all cases, the NMR relaxation data were consistent with the lack of any distribution over T_1 and T_2 relaxation times (Figures S7 and S8).

IR Microscopy (IRM) Measurements. For IR microscopy (IRM) measurements, several large ZIF-11 crystals (batch C) were placed into a cylindrical vacuum cell containing an IR quartz glass window (Starna GmbH). The cell, connected to the gas dosing system, was mounted onto the heatable sample holder under the IR microscope (Hyperion 3000 with Vertex 80v, Bruker Optics). ZIF-11 crystals were activated at 393 K for at least 10 h.

Several individual ZIF-11 crystals were selected for uptake measurements at 298 ± 1 K using the IR microscope visual mode. This temperature, within uncertainty, is the same as that used in most of the PFG NMR measurements. The crystals were exposed to step changes in the surrounding gas-phase concentration, and time dependences of the IR signals of ethane and ethylene inside the monitored crystals were recorded separately for each crystal.

Single-Component Volumetric Gas Sorption Measurements. Single-component transport diffusivities of ethane and ethylene were measured using HPVA-II (Micromeritics) at 296 K with an equilibrium criterion of 0.03 mbar/min for 400 min. Approximately 20 mg of ZIF-11 crystals (batch C) resulting in a thin crystal bed was used to minimize bed diffusion resistance. Samples were activated at 403 K under vacuum prior to measurements. The transport diffusivities were obtained from fitting the measured uptake curves by the corresponding solution of the second Fick's law (eqs S1 and S2), as discussed in Supporting Information.

RESULTS AND DISCUSSION

Figure 2 shows examples of the measured PFG NMR attenuation curves at 296 K for ethane and ethylene in the ZIF-11 samples loaded with a single sorbate (Figure 2A,B) or ethane/ethylene mixture (Figure 2C). The sorbate loading pressure for the data in Figure 2A (0.8 bar) is approximately the same as the highest loading pressure used in the reported below IR microscopy and volumetric uptake studies. Figure 2B presents the corresponding PFG NMR data for the highest sorbate loading pressure used (9.1 bar). Figure 2C shows examples of the PFG NMR attenuation curves for the approximately equimolar gas mixture at the total loading pressure of 2.3 bar. Additional representative examples of the measured PFG NMR attenuation curves for ethane and ethylene as single sorbates at the lowest and intermediate loading pressures at 296 K can be seen in Figure S9A,B, respectively. Furthermore, Figure S9C shows PFG NMR attenuation curve at 296 K for a mixture of ethane and ethylene at a higher sorbate loading than in Figure 2C. All data in Figures 2 and S9 were measured with small crystal batches (A and B), and no difference was observed between the corresponding diffusion data for these batches, within uncertainty.

The measured PFG NMR attenuation curves in all studied batches show a monoexponential behavior (i.e., linear in the semilogarithmic presentation of Figures 2 and S9) with respect to q^2 in agreement with eq 1. Such an observation indicates that for each sample at any measured diffusion time there is a single self-diffusivity for each studied sorbate (ethane or ethylene). This diffusivity can be assigned to the molecules diffusing inside the ZIF-11 crystals, as any signal coming from

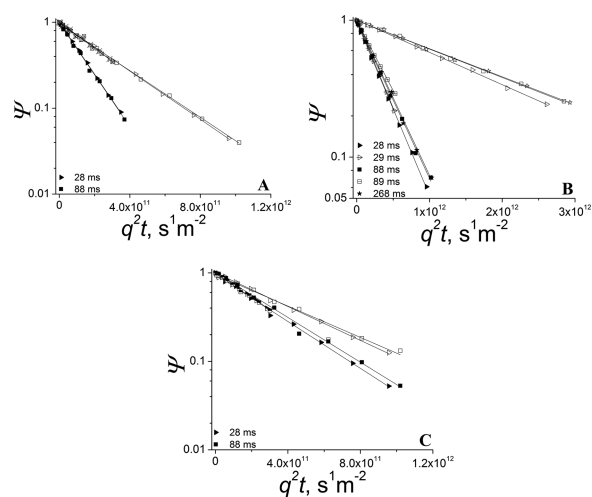


Figure 2. Examples of ^{13}C PFG NMR attenuation curves measured at 17.6 T for ZIF-11 loaded with ethane (filled symbols) and/or ethylene (hollow symbols) at 296 K. The measurements were performed for pure gases at the loading pressures of 0.8 bar (A) and 9.1 bar (B), as well as for the approximately equimolar gas mixture at the total loading pressure of 2.3 bar (C). The corresponding sorbate concentrations can be found in Table 1. Also shown for comparison are the results of the additional PFG NMR measurements that were performed using ^1H nuclei at 17.6 T (open symbols with a horizontal dash for ethane in (B)) and ^{13}C at 14 T (empty symbols with crosses for ethylene in (A) and half-filled symbols for ethane in (C)). Measurements were performed at different diffusion times shown in the figure. The solid lines represent the results of least-square fitting using eq 1. The data were measured with the small crystal batches.

the molecules diffusing in the gas phase of the sample was attenuated away already at the smallest gradient strength used in measurements. Results of least-squares fitting of the measured PFG NMR attenuation curves using eq 1 are shown in Figure 3 and Tables S4 and S5. In addition to the intra-ZIF diffusivities, Tables S4 and S5 also show the corresponding values of root MSDs calculated using eq 2. It is seen in the tables that the root MSDs are significantly smaller than the average size of the studied ZIF-11 crystals (4.5, 3.1, and 100 μm from Table S1). Hence, the influence of

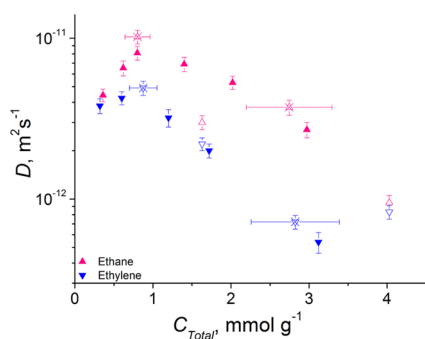


Figure 3. Intracrystalline self-diffusivities of ethane and ethylene measured by PFG NMR in ZIF-11 beds for the smallest diffusion times at 296 K as a function of the total sorbate concentration of ethane and ethylene in ZIF-11 crystals. Filled symbols and empty symbols with crosses show data for the single sorbates in the small (batches A and B) and large (batch C) ZIF-11 crystals, respectively. Hollow symbols show data for the samples with the approximately equimolar ethane/ethylene mixtures in the small ZIF-11 crystals (batches A and B).

any effects at the external surface of ZIF-11 crystals on the measured diffusivities is expected to be small or nonexistent. In agreement with this expectation, the diffusivities in Tables S4 and S5 for the same sorbate loading are independent of the diffusion time, within uncertainty, for the smallest and intermediate diffusion times used in a particular measurement. However, slightly lower diffusivities were measured in some cases (sorbate loadings of ≤ 1.2 mmol/g) in the small crystal batches (A and B) at the largest diffusion times used (Table S4). This observation can be attributed to reflections of molecules diffusing inside the smallest crystals in the samples from the external crystal surface. Owing to a relatively broad crystal size distribution in the small crystal batches (Figure S2), it was not possible to quantitatively analyze the influence of the external crystal surface on the measured diffusivities in the same way as it was done, for example, in ref 8.

Our data in Figure 3 and Table S4 show that, overall, there is a good consistency between the self-diffusivities measured for the small crystal batches (A and B) at the smallest diffusion time and the self-diffusivities measured for batch C at the same or comparable sorbate loadings (compare filled symbols and empty symbols with crosses in Figure 3). The observed maximum difference between the corresponding self-diffusivities measured at comparable sorbate loadings does not exceed 25%. This difference can be due to the presence of some particularly small crystals, which might lead to a slight reduction in the measured diffusivities in the small crystal batches even at the smallest diffusion time used. Such diffusivity reduction can happen because of the restricted nature of diffusion in a small number of the smallest crystals in batches A and B.

The data in Tables S4 and S5 show that the diffusivities measured with ^1H at 17.6 T, ^1H at 14 T, and ^{13}C at 14 T coincide, within experimental uncertainty, with the corresponding diffusivities measured in the same samples and at the same diffusion times using ^{13}C at 17.6 T. Such consistency in the results confirms the absence of any measurement artifacts under our experimental conditions.

It is seen in Figure 3 that at low sorbate loadings there is a trend of increasing sorbate self-diffusivities with increasing sorbate concentration in ZIF-11 for each type of measured samples, i.e., samples loaded with pure ethane and pure ethylene. Such a trend had been previously observed for the diffusion of ethane as single sorbate in ZIF-11 crystals and can be attributed to the expectation that the lowest free energy sites in ZIF-11 with the largest residence times corresponding to lowest self-diffusivities will be occupied first.²² Such a trend was previously observed for zeolites and other microporous materials at small sorbate concentrations comparable with the concentrations of the lowest free energy sites.²⁹ Furthermore, it is seen in Figure 3 that at higher sorbate loadings there is a trend of decreasing sorbate self-diffusivity with increasing total concentration of sorbate molecules in ZIF-11 for each type of the studied samples, i.e., samples loaded with pure ethane, pure ethylene, and ethane/ethylene mixture. This trend had been previously observed for the diffusion of different gaseous sorbates in ZIF-11,^{8,11,22} as well as for the diffusion of different sorbates in other types of microporous materials.^{29,33} Such concentration dependence in ZIF-11 can originate from a higher extent of mutual hindrance of diffusing molecules at higher sorbate concentrations²⁹ and/or from a reduction of the framework flexibility with increasing sorbate concentration, as

was suggested for the ethane diffusion in ref 22 and will be discussed in more detail below.

Figure 3 shows that for all studied sorbate concentrations, except for the lowest one, the self-diffusivities of ethane in the single-sorbate samples are larger than the corresponding self-diffusivities of ethylene at the same or comparable sorbate concentrations. This is an unexpected result due to the larger size of ethane than that of ethylene. Furthermore, for the single-sorbate samples, the diffusivity ratio of ethane to ethylene increases as the sorbate concentration increases (Table S6). These data suggest that there is an interaction between ethylene molecules and the ZIF-11 framework that hinders the self-diffusion process more than the corresponding ethane/framework interaction. Although the nature of this ZIF-11/ethylene interaction is unclear, it is known that olefins can interact stronger with microporous solids than paraffins. In particular, the interaction of carbon–carbon double bond of olefins with open metal sites of MOFs can lead to stronger olefin/MOF than that of paraffin/MOF interaction.³⁴ We hypothesize that ethylene/framework interaction can reduce the maximum and/or effective aperture size in ZIF-11 by reducing the framework flexibility. In particular, such an interaction can reduce the linker flexibility at the pore aperture even at small or intermediate ethylene loadings. A similar linker flexibility reduction effect was previously suggested under conditions of high ethane loadings in ZIF-11.²² To get a better understanding of the anomalous relationship between the ethane and ethylene intracrystalline diffusivities, the diffusion of ethane/ethylene mixtures in ZIF-11 was also investigated by PFG NMR. The measured ethane and ethylene diffusivities in the mixed-sorbate samples can be seen in Figure 3 (hollow symbols). The data in the figure indicate that the diffusivity of ethane is substantially reduced when a fraction of ethane in the sample is substituted by ethylene. This observation indicates that the presence of ethylene is slowing down the self-diffusion of ethane in ZIF-11 crystals. This is consistent with our interpretation of the anomalous relationship for ethane and ethylene intracrystalline self-diffusivities in ZIF-11 beds based on the diffusion-hindering effect of ethylene.

The intra-ZIF self-diffusivities of ethane and ethylene resulting from PFG NMR measurements in the small crystal batches are presented as a function of temperature in Figure 4 and Tables 2 and 3. It is seen in Figure 4 and Tables 2 and 3

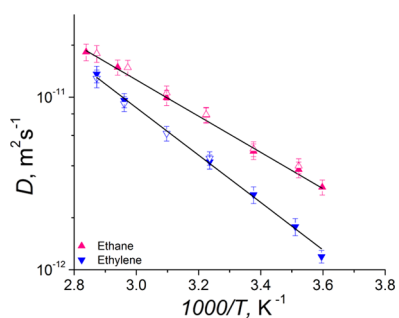


Figure 4. Temperature dependence of the intracrystalline self-diffusivities of ethane and ethylene measured by PFG NMR under the conditions of the same or similar intra-ZIF concentrations and MSDs for each sorbate. The diffusion measurements were performed using ¹H (filled symbols) and ¹³C (hollow symbols) resonances. The data were measured with the small crystal batches.

that, within experimental uncertainty, there is no difference between the measured self-diffusivities when using different types of nuclei (¹H and ¹³C) and otherwise the same conditions. This observation indicates the absence of any types of measurement artifacts in the reported diffusivities. In addition to the self-diffusion coefficients, Tables 2 and 3 also show the root MSD values calculated using eq 2.

It is seen in Tables 2 and 3 that for each particular sorbate the root MSD values are the same or similar at different temperatures. This was achieved by selecting different diffusion times for the diffusion measurements performed at different temperatures. Keeping the root MSDs similar for each sorbate and also significantly smaller than the crystal size at all measured temperatures ensures that the measured temperature dependencies of diffusivities are not perturbed by any effects at the external crystal surface. When performing the measurements of the temperature dependence of intra-ZIF diffusivities, it was taken into account that the intracrystalline sorbate concentration in any particular sealed NMR sample, which contains packed ZIF-11 powder and the gas volume above the powder, is a function of temperature. The extent of sorbate redistribution between the intracrystalline (adsorbed) phase and the gas volume of the sample is primarily determined by the heat of adsorption and the magnitude of the temperature change causing the sorbate redistribution. To obtain the diffusion data corresponding to the same or similar intracrystalline sorbate concentration at different temperatures, several PFG NMR samples with different sorbate loadings at 296 K were prepared and measured. The reported data in Figure 4 and Tables 2 and 3 correspond to such condition of the same or similar concentration at different temperatures.

It is seen in Figure 4 that the temperature dependence for each sorbate can be described using the Arrhenius equation

$$D(T) = D_0 \exp\left(-\frac{E_a}{RT}\right) \quad (3)$$

where E_a is the activation energy of diffusion and D_0 is the pre-exponential factor. Least-squares fitting of the data in Figure 4 using eq 3 yields intra-ZIF diffusion activation energies of 20 ± 2 and 26 ± 3 kJ/mol for ethane and ethylene, respectively. The observation of higher activation energy of diffusion for ethylene than for ethane in ZIF-11 further supports our hypothesis about a smaller effective aperture size in ZIF-11 in the presence of ethylene.

To confirm the data obtained for ethane and ethylene diffusion by PFG NMR and to further investigate the anomalous relationship between the diffusivities measured for ethane and ethylene, complementary diffusion measurements were performed by IRM and standard volumetric technique. These measurements were performed at the same or similar conditions as those carried out by PFG NMR. All IRM and volumetric uptake measurements were done with the large crystal batch (batch C). Using this batch allows monitoring sufficiently large signal-to-noise ratios and uptake times for the observation of a gas uptake in a single crystal by IRM and sufficiently long uptake times required for the volumetric uptake measurements.

The IRM was used to measure uptake curves for ethane and ethylene in individual ZIF-11 crystals (examples of uptake curves are presented in Figure S10). The curves were measured for the smallest possible pressure steps (around 0.2 bar), which still allowed getting sufficiently large signal-to-noise ratios.

Table 2. Intracrystalline Self-Diffusivities of Ethane Measured by ^1H and ^{13}C PFG NMR in the Small Crystal Batches of ZIF-11 at Different Temperatures While Keeping the Intra-ZIF Concentrations and Root MSD Value the Same or Similar

intra-ZIF concentration of ethane ^a (mmol/g)	diffusion time (ms)	nuclei type	temperature (K)	D (10^{-12} m ² /s)	root MSD (μm)
2.3	89	^1H	278	3.0 ± 0.3	1.3 ± 0.1
2.2	89	^1H	284	3.8 ± 0.4	1.4 ± 0.1
2.2	88	^{13}C	284	4.0 ± 0.4	1.4 ± 0.1
2.0	89	^1H	296	4.9 ± 0.5	1.6 ± 0.1
2.0	88	^{13}C	296	5.0 ± 0.5	1.6 ± 0.1
1.8	29	^1H	310	7.9 ± 0.8	1.2 ± 0.1
1.8	28	^{13}C	310	7.9 ± 0.8	1.2 ± 0.1
2.2	29	^1H	323	10.0 ± 1.0	1.3 ± 0.1
2.2	28	$^{13}\text{C}^b$	323	10.6 ± 1.0	1.3 ± 0.1
1.8	19	^1H	340	14.9 ± 1.5	1.3 ± 0.1
1.8	18	$^{13}\text{C}^b$	336	14.8 ± 1.5	1.3 ± 0.1
1.9	19	^1H	352	18.3 ± 2.0	1.4 ± 0.1
1.9	18	$^{13}\text{C}^b$	348	17.9 ± 2.0	1.4 ± 0.1

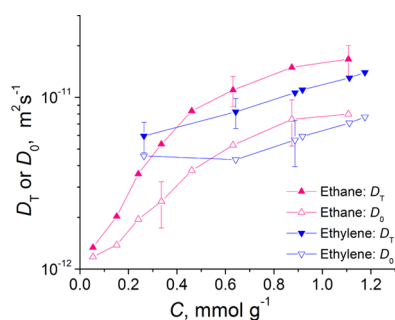
^a20% experimental uncertainty. ^bMeasured at 14 T (all other data measured at 17.6 T).

Table 3. Intra-ZIF Diffusivities of Ethylene Measured by ^1H and ^{13}C PFG NMR in the Small Crystal Batches of ZIF-11 at Different Temperatures While Keeping Intra-ZIF Concentrations and Root MSD Value the Same or Similar

intra-ZIF concentration of ethylene ^a (mmol/g)	diffusion time (ms)	nuclei type	temperature (K)	D (10^{-12} m ² /s)	root MSD (μm)
1.9	89	^1H	278	1.2 ± 0.1	0.80 ± 0.04
1.8	79	^1H	285	1.8 ± 0.2	0.92 ± 0.05
1.7	69	^1H	296	2.7 ± 0.3	1.1 ± 0.1
2.3	29	^1H	309	4.2 ± 0.4	0.86 ± 0.04
2.3	28	$^{13}\text{C}^b$	309	4.4 ± 0.4	0.86 ± 0.04
2.2	19	^1H	323	6.2 ± 0.6	0.84 ± 0.04
2.2	18	$^{13}\text{C}^b$	323	6.2 ± 0.6	0.80 ± 0.04
1.9	19	^1H	338	9.6 ± 1.0	1.1 ± 0.1
1.9	18	$^{13}\text{C}^b$	338	9.2 ± 0.9	0.98 ± 0.05
1.7	9	^1H	348	14 ± 2	0.86 ± 0.04
1.7	9	$^{13}\text{C}^b$	348	13 ± 2	0.83 ± 0.04

^a20% experimental uncertainty. ^bMeasured at 14 T (all other data measured at 17.6 T).

Using such small pressure steps allowed minimizing an error introduced by the assumption of a constant transport diffusivity (D_T) for each measured uptake curve. The transport diffusivities of each studied sorbate were obtained from the least-square fit of the measured curves by the corresponding solution of second Fick's law, as discussed in detail in the previously reported studies performed by this technique.¹⁴ The resulting transport diffusivities are shown in Figure 5 as a function of the average sorbate concentration during the uptake curve measurement. It is seen in the figure that, in

**Figure 5.** Transport and corrected diffusivities of ethane and ethylene measured by IRM at 298 K for individual ZIF-11 crystals as a function of an average sorbate concentration.

complete analogy with the self-diffusion data measured by PFG NMR, the transport diffusivities for both sorbates increase with increasing concentration in the measured concentration range of up to around 1.2 mmol/g. Furthermore, Figure 5 shows that at sufficiently high gas concentrations the transport diffusivity of ethane tends to be larger than that of ethylene at the same or comparable sorbate concentration. Such a relationship was also observed for the self-diffusion of ethane and ethylene in ZIF-11 measured with PFG NMR.

To compare the data obtained by IRM and PFG NMR, it should be noted that transport and self-diffusivities, respectively, are directly measured by these two techniques. While transport diffusivity is different from self-diffusivity, it can be used to calculate a corrected diffusivity (D_0) that can be directly compared with the corresponding self-diffusivity.^{29,35} The corrected diffusivities in ZIF-11 were calculated using "Darken equation"^{29,35}

$$D_T = D_0 \frac{d \ln(p)}{d \ln(c)} = D_0 \Gamma \quad (4)$$

where Γ is the thermodynamic factor obtained from the measured adsorption isotherms $c(p)$. The corrected diffusivities are presented in Figure 5. The measured concentration dependencies of the corrected diffusivities in Figure 5 exhibit the same trends as the transport diffusivities: corrected

diffusivities increase with increasing concentration and tend to be higher for ethane than those for ethylene at higher concentrations.

The volumetric technique was used to measure uptake curves for ethane and ethylene in a thin bed of ZIF-11 crystals. To optimize the signal-to-noise ratio in these measurements, the uptake curves were measured for the pressure step between 0 and 0.8 bar, which is significantly larger than that used in the IRM measurements. Fitting of the solution of second Fick's law with a constant diffusivity (eqs S1 and S2) to the measured uptake curves resulted in the transport diffusivities of 5.7×10^{-12} and 4.1×10^{-12} m²/s for ethane and ethylene, respectively, at the average sorbate concentration of around 0.6 mmol/g. Equation 4 was applied to calculate the corresponding corrected diffusivities, which were found to be 7.5×10^{-12} and 5.4×10^{-12} m²/s for ethane and ethylene, respectively.

Figure 6 compares the self-diffusion data measured by PFG NMR with the corrected diffusivities obtained from the IRM

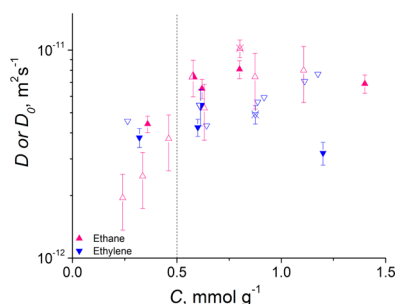


Figure 6. Comparison of the self-diffusivities and corrected diffusivities measured in ZIF-11 crystals for different mean intracrystalline concentrations of ethane or ethylene. Filled symbols and empty symbols with crosses show the self-diffusivities measured by PFG NMR in small (batches A and B) and large (batch C) ZIF-11 crystals, respectively, at 296 K. Empty symbols show the corrected diffusivities in large (batch C) ZIF-11 crystals measured by IR microscopy at 298 K. Half-filled symbols show the corrected diffusivities in large (batch C) ZIF-11 crystals measured by the volumetric technique at 296 K.

and volumetric uptake measurements for the sorbate concentration range between around 0.2 and 1.4 mmol/g, which was used in all three types of measurements. The results in the figure demonstrate that the IRM and volumetric uptake data are consistent with the PFG NMR data, thus confirming the observation of the anomalous relationship between the ethane and ethylene diffusivities in ZIF-11 at the intracrystalline gas concentrations larger than around 0.5 mmol/g. This concentration is indicated by the dotted line in Figure 6. All of the reported above diffusion data suggest that there is a specific interaction between ethylene molecules and the ZIF-11 framework that slows down the diffusion process by reducing the framework flexibility (linker reorientation) and the related effective aperture size in ZIF-11 crystals.

The mechanism to explain the anomalous relationship between the molecular size and diffusivity of ethane and ethylene inside ZIF-11 crystals is not yet fully understood and further structural analyses may be required in addition to computational efforts, which are beyond the scope of this study. In particular, changes in the linker flexibility can be investigated by monitoring shifts in the Zn–N vibration frequency via IR spectroscopy, as recently discussed in ref 36.

In future studies, we will try to extend the spectral range of our IRM setup to enable monitoring such frequency shifts. Previously published data indicate that the interaction between ethylene and ZIF-7 framework (containing benzimidazole linkers) through CH $\cdots\pi$ -type interactions with the linkers can cause geometrical distortion of the ZIF cage entrance and hinder the sorption of ethylene molecules.³⁷ However, in the presence of ethane, weaker van der Waals complex with the linker can form.³⁷ Such a complex is not expected to lead to any significant cage entrance distortions. We believe that a similar situation can also occur in ZIF-11 crystals.

CONCLUSIONS

PFG NMR was used to measure intracrystalline self-diffusivities of ethane and ethylene in ZIF-11 crystals. For selected matching experimental conditions, the self-diffusion measurements were performed using different nuclei types (¹³C and ¹H) and different magnetic field strengths (14 or 17.6 T). The diffusion data was observed to be independent, within uncertainty, of the field and nuclei type, which rules out any potential measurement artifacts in the reported studies. For diffusion in ZIF-11 crystals loaded with a single sorbate at the same or similar concentration larger than 0.5 mmol/g, it was observed that, despite the larger size of ethane than that of ethylene, the intracrystalline self-diffusivity of ethylene is smaller than the corresponding self-diffusivity of ethane at the same temperature. In addition, the activation energy of intra-ZIF diffusion was found to be larger for ethylene than for ethane. It was also observed that replacing a fraction of ethane by ethylene in ZIF-11 crystals leads to a decrease in the ethane diffusivity. To confirm the observed by PFG NMR anomalous relationship between the ethane and ethylene diffusivities in ZIF-11, additional measurements were performed using IR microscopy and volumetric uptake technique. A good agreement between the corrected diffusivities obtained by these two techniques with the self-diffusion data measured by PFG NMR allowed ruling out measurement artifacts under our experimental conditions. All of the reported diffusion data show an anomalous relationship between the sorbate size and diffusivity, as well as diffusion activation energy in ZIF-11. This anomalous relationship is tentatively explained by the existence of a specific interaction between ethylene molecules and the ZIF-11 framework that slows down the intracrystalline diffusion of ethylene and also the intracrystalline diffusion of ethane molecules if the latter molecules are present inside the crystals. The main effect of such ethylene/framework interaction can be a reduction in the linker flexibility that reduces the maximum and/or effective aperture size in ZIF-11. It is important to note that this work is limited to diffusion studies, which could not fully uncover the nature of framework changes in ZIF-11 in the presence of guest molecules causing the observed diffusion behavior.

Since ZIFs can potentially be used in membrane-based separations of ethane/ethylene mixtures, it would be interesting to investigate the diffusion of these gases in ZIF-11-based membranes. Such studies are currently performed by the authors of this work and will be reported in the near future.

ASSOCIATED CONTENT

Supporting Information

The Supporting Information is available free of charge on the ACS Publications website at DOI: 10.1021/acs.jpcc.9b03933.

Ball-and-stick model of ZIF-11 (Figure S1); histogram (Figure S2); powder XRD pattern (Figure S3); single-component adsorption isotherms (Figure S4); ^{13}C NMR spectra (Figure S5); ^1H NMR spectra (Figure S6); ^{13}C NMR relaxation curves (Figure S7); ^1H NMR relaxation curves (Figure S8); ^{13}C PFG NMR attenuation curves (Figure S9); uptake curves (Figure S10); mean size of ZIF-11 crystals (Table S1); T_1 and T_2 NMR relaxation times (Tables S2 and S3); PFG NMR diffusion data (Tables S4 and S5); and ratio of the self-diffusivities (Table S6) (PDF)

AUTHOR INFORMATION

Corresponding Author

*E-mail: svasenkov@che.ufl.edu.

ORCID

Ryan P. Lively: 0000-0002-8039-4008

Sergey Vasenkov: 0000-0002-8619-0612

Notes

The authors declare no competing financial interest.

ACKNOWLEDGMENTS

The authors are grateful for the financial support of this work by NSF (CBET awards No. 1510411 and No. 1510442). A portion of this work was performed in the McKnight Brain Institute at the National High Magnetic Field Laboratory's AMRIS Facility, which is supported by the National Science Foundation Cooperative Agreement No. DMR-1157490 and the State of Florida. This work was supported, in part, by an NIH award, S10RR031637, for magnetic resonance instrumentation. The authors thank Dr. Brian Pimentel for the schematic of ZIF-11.

REFERENCES

- (1) Pimentel, B. R.; Parulkar, A.; Zhou, E.-k.; Brunelli, N. A.; Lively, R. P. Zeolitic Imidazolate Frameworks: Next-Generation Materials for Energy-Efficient Gas Separations. *ChemSusChem* **2014**, *7*, 3202–3240.
- (2) Park, K. S.; Ni, Z.; Côté, A. P.; Choi, J. Y.; Huang, R.; Uribe-Romo, F. J.; Chae, H. K.; O'Keeffe, M.; Yaghi, O. M. Exceptional Chemical and Thermal Stability of Zeolitic Imidazolate Frameworks. *Proc. Natl. Acad. Sci. U.S.A.* **2006**, *103*, 10186–10191.
- (3) Banerjee, R.; Phan, A.; Wang, B.; Knobler, C.; Furukawa, H.; O'Keeffe, M.; Yaghi, O. M. High-Throughput Synthesis of Zeolitic Imidazolate Frameworks and Application to CO_2 Capture. *Science* **2008**, *319*, 939–943.
- (4) Thompson, J. A.; Blad, C. R.; Brunelli, N. A.; Lydon, M. E.; Lively, R. P.; Jones, C. W.; Nair, S. Hybrid Zeolitic Imidazolate Frameworks: Controlling Framework Porosity and Functionality by Mixed-Linker Synthesis. *Chem. Mater.* **2012**, *24*, 1930–1936.
- (5) Phan, A.; Doonan, C. J.; Uribe-Romo, F. J.; Knobler, C. B.; O'Keeffe, M.; Yaghi, O. M. Synthesis, Structure, and Carbon Dioxide Capture Properties of Zeolitic Imidazolate Frameworks. *Acc. Chem. Res.* **2010**, *43*, 58–67.
- (6) Zhang, C.; Lively, R. P.; Zhang, K.; Johnson, J. R.; Karvan, O.; Koros, W. J. Unexpected Molecular Sieving Properties of Zeolitic Imidazolate Framework-8. *J. Phys. Chem. Lett.* **2012**, *3*, 2130–2134.
- (7) Chen, B.; Xiang, S.; Qian, G. Metal-Organic Frameworks with Functional Pores for Recognition of Small Molecules. *Acc. Chem. Res.* **2010**, *43*, 1115–1124.
- (8) Forman, E. M.; Pimentel, B. R.; Ziegler, K. J.; Lively, R. P.; Vasenkov, S. Microscopic Diffusion of Pure and Mixed Methane and Carbon Dioxide in ZIF-11 by High Field Diffusion NMR. *Microporous Mesoporous Mater.* **2017**, *248*, 158–163.

(9) Parkes, M. V.; Demir, H.; Teich-McGoldrick, S. L.; Sholl, D. S.; Greathouse, J. A.; Allendorf, M. D. Molecular Dynamics Simulation of Framework Flexibility Effects on Noble Gas Diffusion in HKUST-1 and ZIF-8. *Microporous Mesoporous Mater.* **2014**, *194*, 190–199.

(10) Pusch, A.-K.; et al. NMR Studies of Carbon Dioxide and Methane Self-Diffusion in ZIF-8 at Elevated Gas Pressures. *Adsorption* **2012**, *18*, 359–366.

(11) Forman, E. M.; Baniani, A.; Fan, L.; Ziegler, K. J.; Zhou, E.; Zhang, F.; Lively, R. P.; Vasenkov, S. Ethylene Diffusion in Crystals of Zeolitic Imidazole Framework-11 Embedded in Polymers to Form Mixed-Matrix Membranes. *Microporous Mesoporous Mater.* **2019**, *274*, 163–170.

(12) Mueller, R.; Zhang, S.; Zhang, C.; Lively, R. P.; Vasenkov, S. Relationship between Long-Range Diffusion and Diffusion in the ZIF-8 and Polymer Phases of Mixed-Matrix Membrane by High Field NMR Diffusometry. *J. Membr. Sci.* **2015**, *477*, 123–130.

(13) Mueller, R.; Hariharan, V.; Zhang, C.; Lively, R.; Vasenkov, S. Relationship between Mixed and Pure Gas Self-Diffusion for Ethane and Ethene in ZIF-8/6FDA-DAM Mixed-Matrix Membrane by Pulsed Field Gradient NMR. *J. Membr. Sci.* **2016**, *499*, 12–19.

(14) Chmelik, C.; Bux, H.; Caro, J.; Heinke, L.; Hibbe, F.; Titze, T.; Kärger, J. Mass Transfer in a Nanoscale Material Enhanced by an Opposing Flux. *Phys. Rev. Lett.* **2010**, *104*, No. 085902.

(15) Chmelik, C.; Kärger, J. The Predictive Power of Classical Transition State Theory Revealed in Diffusion Studies with MOF ZIF-8. *Microporous Mesoporous Mater.* **2016**, *225*, 128–132.

(16) Berens, S.; Chmelik, C.; Hillman, F.; Kärger, J.; Jeong, H.-K.; Vasenkov, S. Ethane Diffusion in Mixed Linker Zeolitic Imidazolate Framework-7-8 by Pulsed Field Gradient NMR in Combination with Single Crystal IR Microscopy. *Phys. Chem. Chem. Phys.* **2018**, *20*, 23967–23975.

(17) Pantatosaki, E.; Megariotis, G.; Pusch, A.-K.; Chmelik, C.; Stallmach, F.; Papadopoulos, G. K. On the Impact of Sorbent Mobility on the Sorbed Phase Equilibria and Dynamics: A Study of Methane and Carbon Dioxide within the Zeolite Imidazolate Framework-8. *J. Phys. Chem. C* **2012**, *116*, 201–207.

(18) Nordin, N. A. H. M.; Ismail, A. F.; Mustafa, A.; Murali, R. S.; Matsuura, T. The Impact of ZIF-8 Particle Size and Heat Treatment on CO_2/CH_4 Separation Using Asymmetric Mixed Matrix Membrane. *RSC Adv.* **2014**, *4*, 52530–52541.

(19) Bux, H.; Liang, F.; Li, Y.; Cravillon, J.; Wiebcke, M.; Caro, J. Zeolitic Imidazolate Framework Membrane with Molecular Sieving Properties by Microwave-Assisted Solvothermal Synthesis. *J. Am. Chem. Soc.* **2009**, *131*, 16000–16001.

(20) Assfour, B.; Leoni, S.; Seifert, G. Hydrogen Adsorption Sites in Zeolite Imidazolate Frameworks ZIF-8 and ZIF-11. *J. Phys. Chem. C* **2010**, *114*, 13381–13384.

(21) Sánchez-Láinez, J.; Zornoza, B.; Mayoral, Á.; Berenguer-Murcia, Á.; Cazorla-Amorós, D.; Téllez, C.; Coronas, J. Beyond the H_2/CO_2 Upper Bound: One-Step Crystallization and Separation of Nano-Sized ZIF-11 by Centrifugation and Its Application in Mixed Matrix Membranes. *J. Mater. Chem. A* **2015**, *3*, 6549–6556.

(22) Kortunov, P.; Ni, Z.; Paur, C.; Reyes, S.; Zengel, J. Loading-Dependent Transport Properties of Zeolitic Imidazolate Frameworks Probed by In-Situ PFG NMR. *AIP Conf. Proc.* **2011**, *1330*, 57–60.

(23) Li, J.-R.; Kuppler, R. J.; Zhou, H.-C. Selective Gas Adsorption and Separation in Metal–Organic Frameworks. *Chem. Soc. Rev.* **2009**, *38*, 1477–1504.

(24) Shi, M.; Lin, C. C. H.; Kuznicki, T. M.; Hashisho, Z.; Kuznicki, S. M. Separation of a Binary Mixture of Ethylene and Ethane by Adsorption on Na-ETS-10. *Chem. Eng. Sci.* **2010**, *65*, 3494–3498.

(25) Shi, M.; Avila, A. M.; Yang, F.; Kuznicki, T. M.; Kuznicki, S. M. High Pressure Adsorptive Separation of Ethylene and Ethane on Na-ETS-10. *Chem. Eng. Sci.* **2011**, *66*, 2817–2822.

(26) He, M.; Yao, J.; Liu, Q.; Zhong, Z.; Wang, H. Toluene-Assisted Synthesis of RHO-Type Zeolitic Imidazolate Frameworks: Synthesis and Formation Mechanism of ZIF-11 and ZIF-12. *Dalton Trans.* **2013**, *42*, 16608–16613.

(27) Dvoyashkin, M.; Zang, J.; Yucelen, G. I.; Katihar, A.; Nair, S.; Sholl, D. S.; Bowers, C. R.; Vasenkov, S. Diffusion of Tetrafluoromethane in Single-Walled Aluminosilicate Nanotubes: Pulsed Field Gradient NMR and Molecular Dynamics Simulations. *J. Phys. Chem. C* **2012**, *116*, 21350–21355.

(28) Cotts, R. M.; Hoch, M. J. R.; Sun, T.; Markert, J. T. Pulsed Field Gradient Stimulated Echo Methods for Improved NMR Diffusion Measurements in Heterogeneous Systems. *J. Magn. Reson.* (1969) **1989**, *83*, 252–266.

(29) Kärger, J.; Ruthven, D. M.; Theodorou, D. N. *Diffusion in Nanoporous Materials*; Wiley-VCH Verlag GmbH & Co. KGaA: Weinheim, Germany, 2012.

(30) Kärger, J.; Pfeifer, H.; Heink, W. Principles and Application of Self-Diffusion Measurements by NMR. *Adv. Magn. Reson.* **1988**, *12*, 1–89.

(31) Stejskal, E. O.; Tanner, J. E. Spin Diffusion Measurements: Spin Echoes in the Presence of a Time-Dependent Field Gradient. *J. Chem. Phys.* **1965**, *42*, 288–292.

(32) Callaghan, P. T.; MacGowan, D.; Packer, K. J.; Zelaya, F. O. Influence of Field Gradient Strength in NMR Studies of Diffusion in Porous Media. *Magn. Reson. Imaging* **1991**, *9*, 663–671.

(33) Chmelik, C.; van Baten, J.; Krishna, R. Hindering Effects in Diffusion of CO₂/CH₄ Mixtures in ZIF-8 Crystals. *J. Membr. Sci.* **2012**, *397–398*, 87–91.

(34) Chang, G.; et al. Immobilization of Ag(I) Into a Metal-Organic Framework with -SO₃H Sites for Highly Selective Olefin-Paraffin Separation at Room Temperature. *Chem. Commun.* **2015**, *51*, 2859–2862.

(35) Kärger, J.; Vasenkov, S.; Auerbach, S. M. Diffusion in Zeolites. In *Handbook of Zeolite Science and Technology*; Auerbach, S. M., Ed.; Marcel Dekker, Inc.: New York, 2003; pp 341–422.

(36) Hillman, F.; Jeong, H.-K. Linker-Doped Zeolitic Imidazolate Frameworks (ZIFs) and Their Ultrathin Membranes for Tunable Gas Separations. *ACS Appl. Mater. Interfaces* **2019**, *11*, 18377–18385.

(37) van den Bergh, J.; Gücüyener, C.; Pidko, E. A.; Hensen, E. J. M.; Gascon, J.; Kapteijn, F. Understanding the Anomalous Alkane Selectivity of ZIF-7 in the Separation of Light Alkane/Alkene Mixtures. *Chem. – Eur. J.* **2011**, *17*, 8832–8840.